Molecular Dipole Chains: Excitations and Dissipation

S. W. DeLeeuw and D. Solvaeson

Faculty of Applied Physics, University of Delft, Lorentzweg 1, 2628 C.J. Delft, The Netherlands

Mark A. Ratner*

Department of Chemistry and Materials Research Center, Northwestern University, Evanston, Illinois 60208

Josef Michl*

Department of Chemistry and Biochemistry, University of Colorado, Boulder, Colorado 80301

Received: June 26, 1997; In Final Form: January 28, 1998

As a model for orientational excitation of molecular arrays, we examine the excitation behavior and energy flow patterns in a model system. The model is simply a chain of classical point dipoles with fixed mass center, rotating in a plane containing the intermolecular axis, and interacting by the classical dipole potential. At low energies, the dispersion relation is quite different from that for a phonon system, showing a flat frequency maximum at $k = 0$. Correlation function analysis shows a significant transition from the low-energy regime in which the local dipole motion is predominantly oscillatory (with periodic correlation functions and Fourier components that maximize at a well-defined oscillation frequency), to a high-energy situation in which a Rayleigh peak occurs in the $k = 0$ Fourier component, and finite frequency response occurs only for higher wave vector. Physically, this transition occurs for thermal energy roughly equal to the typical magnitude of the local dipolar interaction. Thus for energies above this transition, the kinetic energies are high enough that the local motion is predominantly rotatory rather than oscillatory. These changes are also seen in the frequency moments and Kirkwood *g*-factors. The simulations show that initial energy deposited in one rotating dipole passes down the chain almost like a solitary wave, reflecting off of the free chain end and then traversing the chain again.

I. Introduction

Synthetic advances, including use of weak interactions and selective dimensional stabilization, have recently produced a number of fascinating extended molecular structural arrays. These structures range from self-assembled films[1−7] exhibiting nonlinear optical properties[5,8] to "molecular tinkertoy" constructions in which rigid or semirigid molecules are used in an attempt to assemble molecular arrays for particular purposes.[9−12] One exciting possibility is the use of these molecular assembly techniques to produce solids with purposefully engineered interactions among specific, appropriately placed molecular substituent groups.[13]

One possible such scheme might involve planar arrays of dipolar molecular species, especially arranged such that their centers cannot move, and locally pivoted in such a way that the rotation of the dipole in the plane is nearly free. A molecular dynamics simulation of a "molecular windmill", carrying a large dipole and driven by a flow of supersonic He gas, has already been completed.[13]

A problem of immediate interest, then, involves the nature of the excitations of such an array of dipoles. We deal here with molecules that can have substantial dipole moments (upwards of 50 D), with relatively large moments of inertia (near 10^{-43} kg M^2). The problem is therefore essentially a classical one, and the true dipolar structure, including its long range, should be taken into account. Additionally, the molecules will interact with one another through the usual steric and Lennard-Jones forces, which can lead to blocking and orientational frustration in densely packed arrays. It is the local decay dynamics of an initially excited dipole and the excitation spectrum and energy loss behavior of such an array that will be studied in this and subsequent papers.

This first paper is devoted simply to the excitations, dispersion and dissipation processes of an array of molecular dipoles, whose centers are fixed, and whose geometry can therefore be completely described by rotation of the dipole around its center. Two such motions can occur: one is the rotation around the axis linking the dipolar centers (conveniently taken as the *z*-axis), as occurs in linear chain species like Ni−(phthalocyanine)−I;[14] here, the *z*-axis projection of the dipole moments vanishes and motion occurs in the (*x*,*y*) plane. The other involves motions in the (*x*,*z*) plane, so that the projection of the dipole moments on the *z*-axis changes in time. We analyze this second case here. We treat these molecules as classical point dipoles interacting only by long-range dipole−dipole interaction.

The collective excitations of such a system are of interest, as are the nature of the dissipation and excitation processes that would be entailed if one molecule is suddenly excited (say by collision with an external probe). In section II, the Hamiltonian of the problem and the low frequency excitation spectrum (analogous to the magnons in the corresponding magnetic problem)[15] are described. In section III, molecular dynamics methods are used to characterize the energy transfer from an initially excited dipole. Section IV describes molecular dynamics (MD) simulations to characterize the correlations and

S1089-5647(97)02089-0 CCC: $15.00
Published on Web 04/28/1998

dynamics in an equilibrium system of these dipoles, and some remarks and speculations appear in section V.

II. Hamiltonian and the Low-Energy Excitations

We consider, then, for simplicity a linear array of equidistant point dipoles rotating in a plane (the (*x*,*z*) plane) that contains the line. The center to center distance of the dipoles is fixed, and each dipole can pivot around its center of mass. The problem can then be described in terms of a local polar angle φ for each dipole. We study a one-dimensional chain of sites.

The Lagrangian of this system can then be written as

$$L = \frac{1}{2\mu^2} I \sum_i \dot{\mu}_i^2 - \sum_{i>j}{}' \left(\frac{\vec{\mu}_i \cdot \vec{\mu}_j}{r_{ij}^3} - \frac{3(\vec{\mu}_i \cdot \vec{r}_{ij})(\vec{\mu}_j \cdot \vec{r}_{ij})}{r_{ij}^5} \right) \quad (1)$$

Here I, $\vec{\mu}_i$, and $\vec{r}_{ij}$ are respectively the moment of inertia, the dipole moment on the ith site, and the distance vector between sites i and j (compare with **A**). If we replace the dipole moment

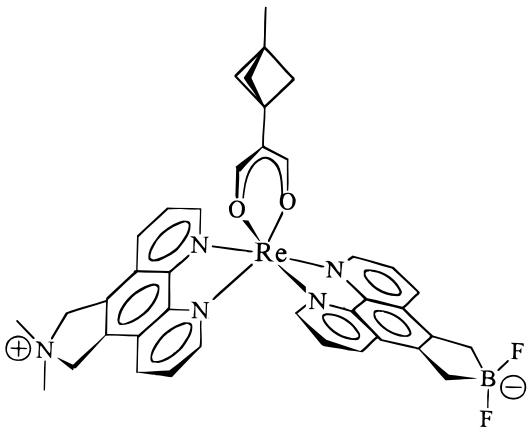

A

vector by its magnitude μ and its rotational angle φ, eq 1 can be written as eq 2.

$$L = {}^1/_2 I \sum_i \dot{\varphi}_i^2 - \frac{\mu^2}{r_o{}^3} \sum_{i>j}{}' \frac{(\sin\varphi_i \sin\varphi_j - 2\cos\varphi_i \cos\varphi_j)}{|i-j|^3} \quad (2)$$

Here we have defined r_o as the (constant) distance between the centers of neighboring dipoles. The Lagrangian equations of motion in the form

$$\frac{\mathrm{d}}{\mathrm{d}t} \frac{\partial L}{\partial \dot{\varphi}_i} = \frac{\partial L}{\partial \varphi_i} \quad (3)$$

then yield equations of motion for the angles, in the form,

$$\ddot{\varphi}_l = -C \sum_{j \neq l}{}' \frac{(\cos\varphi_l \sin\varphi_j + 2\sin\varphi_l \cos\varphi_j)}{|l-j|^3} \quad (4)$$

with the definition:

$$C = \frac{\mu^2}{I r_o{}^3} \quad (5)$$

Solution of eq 4 gives the excitation behavior of the dipole chain. The equations of motion (eq 4) are nonlinear, with no simple analytic solution. In the general case, they can be solved numerically using molecular dynamics—this is discussed in sections III and IV. Here we concern ourselves with the low-energy excitations of this dipolar array.

Clearly, the potential term of the Lagrangian in equation 2 will be minimized when all of the dipoles are parallel along the *z*-axis, so that φ_i vanishes, and cos φ_i is equal to unity. Then the minimum potential can be written as

$$V_{\min} = V(\varphi_i = 0) = -\frac{\mu^2}{r_o{}^3} \sum_{l>j} \frac{1}{|l-j|^3} \qquad \forall i \quad (6)$$

If the chain containing N dipoles is taken as periodic and very long, this gives

$$V_{\min} = -2\,\frac{(N-1)\mu^2}{r_o{}^3}\,\zeta(3) \quad (7)$$

where $\zeta(3) = 1.202\,05$ is the Riemann ζ function.[16] In practice, the sum in eq 6 converges very rapidly, so that the result (eq 7) holds to better than 5% for an eight-site chain.

The low-energy excitations away from this minimum potential can be found by expanding the trigonometric functions in eq 4. When this is done, we obtain the equations of motion for the low-energy excitations as

$$\ddot{\varphi}_l = -C \sum_{j \neq l}{}' \frac{1}{|l-j|^3} \{2\varphi_l + \varphi_j\} \quad (8)$$

Again recognizing the ζ function, this becomes

$$\ddot{\varphi}_l = -4C\,\varphi_l\,\zeta(3) - C \sum_{j \neq l} \frac{1}{|l-j|^3} \varphi_j \quad (9)$$

We now look for periodic excitations, in the form

$$\varphi_l^{(k)} = \mathrm{u}_k \mathrm{e}^{ilk} \mathrm{e}^{i\omega_k t} \quad (10)$$

here, u_k is the characteristic displacement, k is a wave vector, and ω_k is the characteristic frequency. Inserting this ansatz into the equation of motion 9, we obtain

$$-\omega_k^2\,\varphi_l^{(k)} = -4C\zeta(3)\varphi_l^{(k)} - C \sum_{j \neq l}{}' \frac{1}{|l-j|^3}\,\varphi_j^{(k)} \quad (11)$$

Or, equivalently,

$$-\omega_k^2 = -4C\zeta(3) - C \sum_{j \neq l}{}' \frac{1}{|l-j|^3} \mathrm{e}^{ik(j-l)} \quad (12)$$

This form can be simplified if we replace the sum over j by a sum over $l-j$, which we rename m. This yields

$$-\omega_k^2 = -4C\zeta(3) - C \sum_{m \neq 0}{}' |m|^{-3} \mathrm{e}^{-ikm} \quad (13)$$

Equivalently, one could use real functions in the form

$$\omega_k^2 = 4C\zeta(3) + 2C \sum_{m>0}{}' \frac{\cos k\,m}{m^3} \quad (14)$$

This is the dispersion relation for the frequencies of low-energy excitations of the classical linear dipolar chain. Clearly, the zero wave vector solution is given by

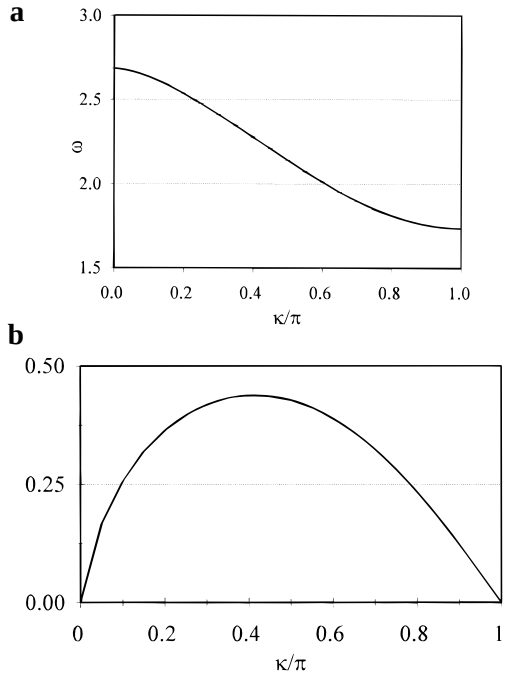

Figure 1. (a) Dispersion curve (eq 14; frequency as a function of wave vector) for low-energy excitations. The maximum energy is reached at zero frequency; the C parameter of eq 14 is set to unity. (b) The group velocity, at which the excitation spreads along the chain (eq 16). Note that v_g is effectively constant over a broad range near $k \cong 0.4\pi$.

$$\omega_0^2 = 6C\zeta(3) \tag{15}$$

For wave vector greater than zero, the solution of (eq 14) can be obtained easily. We present the dispersion spectrum (with $C = 1$) in Figure 1a, and there are several interesting aspects of it. First, notice that the maximum excitation energy is reached at zero frequency. The limits on the wave vector k are $-\pi$ and $+\pi$, and from eq 14, it is clear that ω_k^2 is an even function of k. The dispersion spectrum flattens out to the expected van Hove singularity at π and $-\pi$.[17] Notice how this dispersion relation resembles the optical peak in a Debye-type model of a crystal lattice.[18] This is understandable in terms of the motions of the dipoles: the low-frequency excitations that we are calculating correspond to very small oscillations away from a perfectly parallel arrangement of the dipoles. Whenever a dipole pivots around its center, changes occur in the distance between local positive and negative charges. This is exactly the nature of the excitation involved in the optical band of an ABABABAB Debye chain. Therefore, the similarity of these excitations to the optic excitations in the linear chain is expected.

The actual amplitude of the frequency scales like $\sqrt{C}$, which is to say the inverse square root of the product of the moment of inertia and the cube of the distance between lattice points, as well as the square of the dipole moment. Again, this is sensible: larger moments of inertia will reduce oscillation amplitudes, while increasing r_0 will place the dipoles farther apart, and thus reduce their interaction; so will a reduction in the size of μ.

From the dispersion relation of eq 14, we can obtain the group velocity from

$$v_g = \left|\frac{d\omega(k)}{dk}\right| = \frac{C}{\omega(k)}\sum_{m=l}^{\infty}\frac{\sin km}{m^2} \tag{16}$$

The group velocity in the low energy limit vanishes at $k = 0$ and $k = \pi$ and maximizes near $k = \pi/2$, at a value of $v_g \cong 0.42$ (taking $C = 1$). Actually, the dispersion is fairly flat in the region near $\pi/2$. Figure 1b plots the group velocity (eq 16) in the low-temperature limit. Note that the $k = 0$ and $k = \pi$ excitations have vanishing group velocities.

At very low temperature, the excitations are phonon-like and noninteracting, so that they would pass each other if propagating along the chain. For higher temperatures, the harmonic form of eq 10 is inadequate, and the excitations will then interact.

One would expect to see these low frequency excitations by, for instance, inelastic scattering off of the dipolar chain. More interesting, however, are the structures adopted by the chain (not necessarily at small energies), the nature of the energy sharing process when one rotor is strongly excited, and the energy-dependent correlation and dynamics in the chain.

III. Decay of Initial Excitations: Energy Transfer

One of the most challenging and interesting aspects of the molecular assembly process is preparation of structures that will, in some sense, be electroactive, magnetically active or optically active. The molecular arrays represented by our dipolar chain could, for example, be thought of as energy storage, energy transfer, or electromagnetic conversion systems. To understand this, and also to examine the nature of energy evolution processes within the molecular chain, it is of interest to observe the decay of highly excited, initially localized rotation.

To study the local dynamics, as well as the correlations in the next section, we used molecular dynamics methods for the Lagrangian defined by eq 2. Details of these simulations are outlined in the appendix, where we also define the reduced units used here.

To observe the relaxation of an initially locally excited dipole, we studied a linear chain of 100 dipoles. At the initial time, all the dipoles are aligned and the central dipole is given a large initial kinetic energy. The relatively rapid fall off of the dipole potential suggests that the most important initial decay will be transfer to the next nearest neighbor; subsequent transfer between fairly close-lying dipoles should result in excitations moving along the lattice. Since the chain is finite, with free end boundary conditions, one will also eventually see a Poincaré recurrence and, even before that, one might anticipate that the initial pulse of energy will reflect off the chain ends and return.

Figure 2 shows the evolution of the orientational angle of the different dipoles in the chain, following excitation of dipole 50 (the central dipole) with 10 units of kinetic energy at time zero (units are discussed in the appendix). Figure 2 shows the temporal behavior of the initially excited dipole, its nearest neighbor, and a dipole halfway down the chain toward the end. Two obvious behaviors occur. At very short times, the initially excited dipole oscillates very rapidly, even undergoing complete rotation roughly four times. During this time (up to roughly 10 time units), energy transfer to the neighboring dipoles begins, and they also begin to oscillate. After one time unit, substantial energy transfer to the next neighbor site has occurred; the two sites then both oscillate with a period of roughly 6.4 time units. The motion of the initially excited dipole exhibits a secondary structure, in which every other oscillation is larger. A similar, very much smaller, secondary oscillation is seen in the 49th dipole. After a time of roughly 120 units, the relative amplitudes of the secondary oscillations change, with the 49th dipole exhibiting a larger alternation, and then the oscillations become more structured as more energy is dissipated into the chain.

Dipole 25 shows no initial oscillation at all, since the initial excitation is far away and the dipole potential falls off relatively

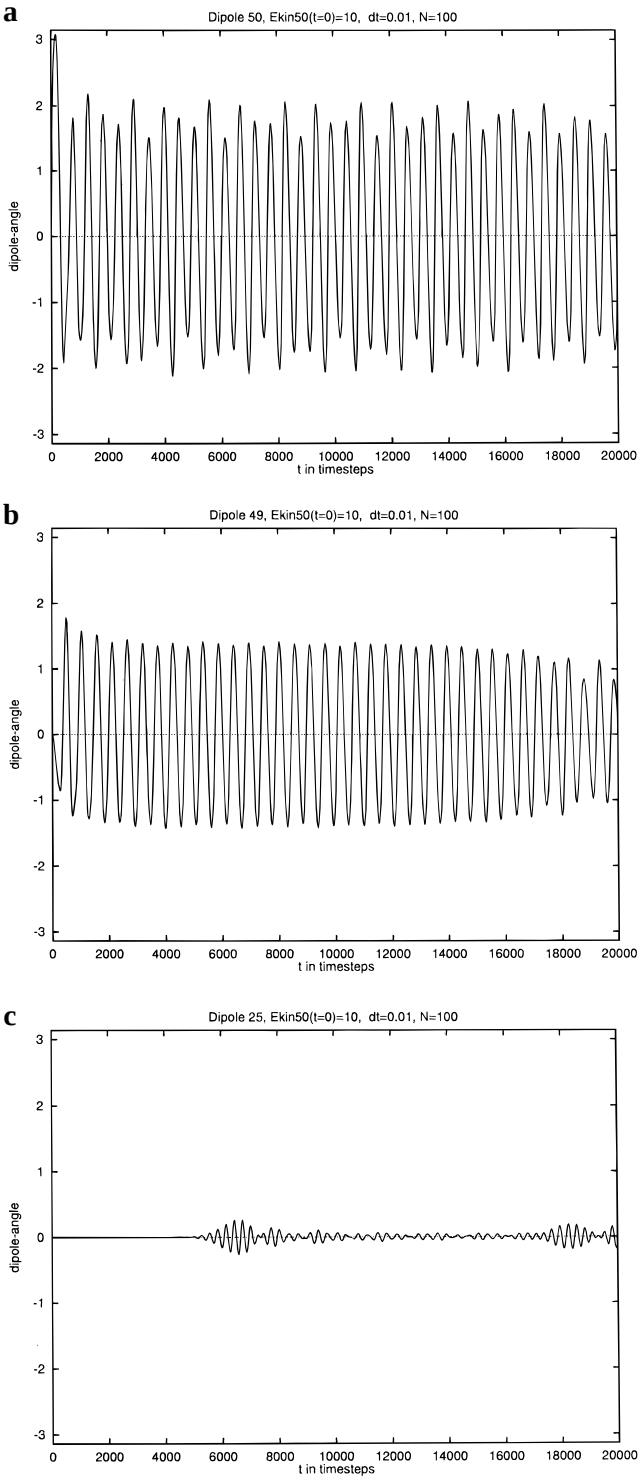

Figure 2. Temporal decay of initial excitation, in a 100 dipole chain. The 50th dipole is originally given angular velocity corresponding to an energy of 10 units, and the angular position of the dipoles for the initially excited dipole, its nearest neighbor, and a dipole halfway towards the end of the chain are shown in (a), (b), and (c), respectively. Note the initial free rotation, which quickly transfers into decaying periodic oscillations on the initial site, the growth of these periodic oscillations on the near-neighbor site, and the long-time, reduced amplitude pulse of excitation halfway down the chain.

quickly. Bursts of excitation are seen at this site, the first occurring at roughly 60 time units. The major pulse seen near 200 time units corresponds to a combination of several excitations, including a dominant one arising from reflection off the end. The secondary oscillation seen at the 25th site shows a frequency substantially higher than the local oscillations seen at the 49th or 50th dipole.

The excitation should travel down the dipole chain at a propagation velocity equal to the group velocity. This is given by eq 16, and maximizes near $k = \pi/4$ where

$$v_g|_{max} = |\frac{d\omega(k)}{dk}| \cong |\frac{\omega(k=0) - \omega(k=\pi/2)}{\pi/2}| \cong \frac{0.64}{1.57} = 0.41 \quad (16a)$$

Numerically, from Figure 2, the velocity of propagation is the distance (25 lattice sites) divided by the time (60 units), or $25/60 = 0.42$. Thus the excitation indeed travels at group velocity. At very low temperatures, the dispersion relation of eq 14 holds, and we find

$$v_g = \frac{C}{\sqrt{\omega^2(k)}} \sum_{m=1} \frac{\sin(km)}{m^2} \quad (16b)$$

This vanishes for $k = 0$, and maximizes in the center of the band, attaining the value $v_g \cong 0.43$ for $k = \pi/4$. For finite temperatures, the simulation results show that the harmonic expansion and the simple dispersion relaxation of eq 14 fail.

Note also that oscillation frequency, as shown by the six largest oscillations, is (from the figure) $12\pi/(71 - 66) \cong 2.5$; this is very close to the maximum frequency of $\omega_o \cong 2.7$ (Figure 1) from the dispersion relation.

When the initial excitation energy is smaller, similar behavior is seen. The initial end-over-end rotation is never attained for this reduced local kinetic energy, so that the very fast, large amplitude oscillations at short times are missing. One still sees the relatively rapid transfer to the neighbor dipole no. 49 (in this case it is slightly faster), and the local oscillations with a period of roughly six time units. With the lower kinetic energy, the excitation of the 25th dipole occurs slightly earlier, with slightly smaller amplitude, and with larger energy: this may reflect the increased relative efficiency of transfer at very short times.

IV. Energy Flow and Statistical Behavior Correlation Functions

In most physical situations, the molecular assembly is subject to thermal forces, and one anticipates that, in addition to the local dynamics described in section III, thermal correlations will be relevant to the behavior of the molecular material. Therefore, in this section we study the dipolar correlation functions and their decays for differing temperatures and frequencies. Because these simulations are carried out in the microcanonical ensemble, intermode energy exchange is inefficient at low kinetic temperatures. Thus substantial fluctuations in the computed kinetic energy distribution are expected (shown in Figure 8, vide infra).

The fundamental dynamics of the assembly is indexed by the time correlation functions, defined by

$$C'(t) = \langle A(0)A^*(t)\rangle \quad (17)$$

$$C(t) = C'(t)/C'(0) \quad (18)$$

Here choice of the time dependent dynamical variable A defines the appropriate time correlation function. We are particularly interested in two time correlation functions: the first is C_1, the correlation function of the dipoles themselves, defined by

$$A(t) = \vec{\mu}(t) \quad (19)$$

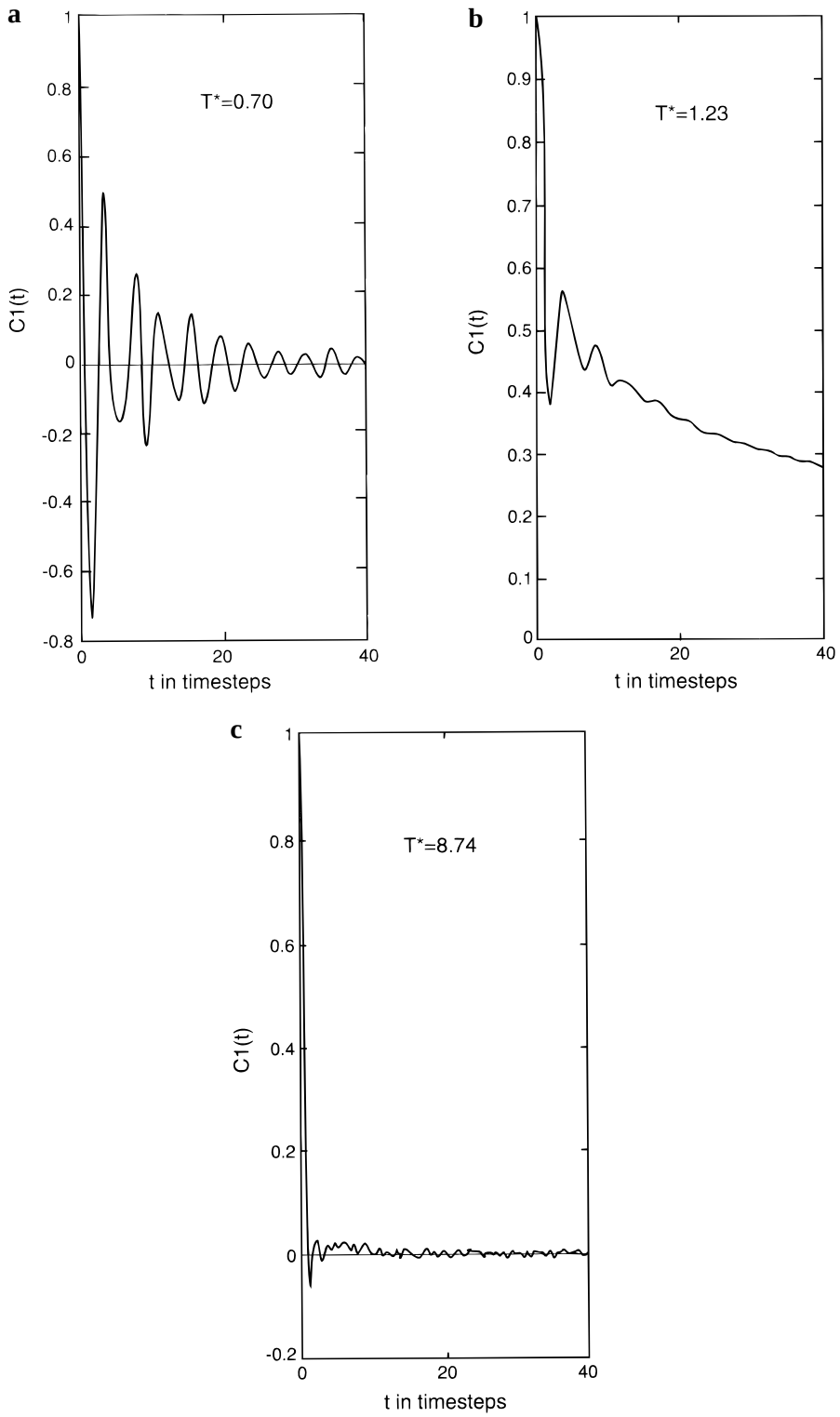

Figure 3. Dipole orientation correlation functions for the 100 particle chain. Note that the long-range correlations in time seen for small temperatures ($T^* \approx 70$, (a)) are substantially reduced for higher temperatures ($T^* \approx 1.23$, (b)) and essentially disappear at very high temperatures ($T^* \approx 8.34$, (c)). The long-time tail in (b) shows remaining correlations that remain until quite high thermal energy.

The second is C_2, the correlation function of the Fourier densities, defined by

$$A(t) = \sum_{l=1}^{N} \begin{pmatrix} \mu_{l,x}(t) \exp(ikx_l) \\ \mu_{l,y}(t) \exp(ikx_l) \end{pmatrix} \tag{20}$$

The correlation functions C_1 and C_2 describe orientational diffusion and polarization density respectively. Since the rotating dipoles describe a fluctuating polarization, they should characterize an optical spectrum, proportional to

$$D(\omega) = \frac{1}{\pi}\int_0^\infty \frac{\langle \mu_i(t)\mu_i(0)\rangle}{\langle \vec{\mu}_i^{\,2}\rangle} \cos(\omega t)\, \mathrm{d}t \tag{21}$$

and can be obtained from the MD simulations.

Clearly, from the definition of eq 17, these correlation functions must be unity at short times, and vanish in the long

time, statistical limit. Also, both C_1 and C_2 must be real (this is a good check of the computational technique for C_2).

The calculations reported here use units in which $I = 1$, $r_0 = 1$, and $\mu = 1$. We use an energy comparison with $\epsilon = \mu^2/r_o^3$, the typical magnitude of the dipolar interaction, to define the reduced temperature by

$$T^* = \frac{k_B T}{\epsilon} = \frac{I r_o^3}{N \mu^4} \sum \dot{\vec{\mu}}_i^2 \qquad (22)$$

(with k_B equal to Boltzmann's constant). We see that for T^* of the order of unity, the system will change from one in which the local dipolar interactions are larger than thermal energy to one in which they are smaller. One might, then, expect an instability or change in behavior at this temperature (no actual phase transitions can occur in this one-dimensional system).

Figure 3 shows the dipole correlation function for three different values of the temperature. It is quite clear that, at low temperatures, there are stable oscillations of the dipole correlation function over the first few dozen time units. At higher temperatures, these oscillations disappear more rapidly, and at very high temperatures they are replaced by statistical noise after a very short (less than five units) time. This is clearly the effect of thermal bombardment: the correlations are lost to random local fluctuations caused by the kinetic energy (elevated temperature).

The correlations are probably clearer in the spacial Fourier component correlation functions. Figure 4 shows the zero wave vector correlation functions. For low temperatures (Figure 4a), we again see clear oscillations extending to rather long times. As the temperature is raised, the initial correlations disappear very quickly, although the overall relaxation behavior is relatively slow for $T^* = 1.23$. This decay becomes statistical over very short times (less than five time units) at the highest temperature investigated, $T^* = 8.74$. At higher wave vectors, corresponding to larger phase differences between neighboring sites, periodicity occurs even at higher temperatures: for example, Figure 5b shows that at a momentum of 0.64π there are oscillations even at the higher temperature over long times, of course these remain clearer at lower temperatures, as is seen from Figure 5a. In most cases for $k \neq 0$, the polarization $A(t)$ decays are oscillatory, so that C_2 drops below zero for some times.

The frequency Fourier transforms clearly show the change from low temperature to high temperature behavior. Figure 6 shows the Fourier analysis of the zero wave vector correlation function. It changes dramatically from the single resonance peak at low temperatures to a spectrum dominated by a zero frequency (Rayleigh-like) peak for $T^* > 1.23$. The half-width of the Rayleigh line is small, $\Delta\omega \sim 0.2$, reflecting the slow diffusion of the excitation down the chain. At higher wave vectors (Figure 7), the resonance peak moves lower for the low-temperature sample (thermal smearing of the potential produces, effectively, a lower local restoring force). At higher temperature, a finite frequency response structure begins to develop, in roughly the same range (1.7 frequency units) for wave vector value 0.6π. Again, this corresponds to more local interactions, where collective, local oscillations will remain even when the long-range oscillations have been thermally smeared.

The thermal fluctuations within the system, corresponding to energy fluctuations from microcanonical simulation, index the growing disorder. Figure 8 shows the thermal behavior; notice that the thermal fluctuations maximize for $T^* \approx 1.7$, and

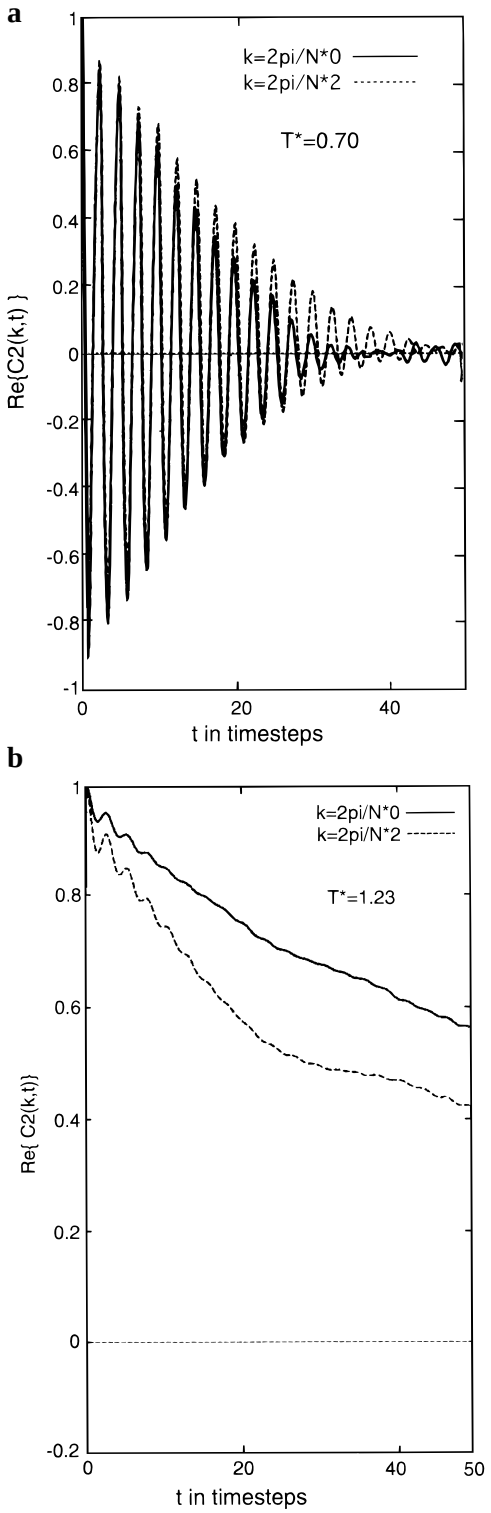

Figure 4. Fourier component time correlation functions. The $k = 0$ results are shown in (a) and (b) for increasing values of the temperature ($T^* \approx 0.70$, 1.23). Increasing thermal energy decreases the temporal range of strong correlations.

that they are far larger for $T^* \approx 1.23$ than for $T^* \approx 0.70$. The T^* fluctuations are quite small in general (proportional to $N^{-1/2}$). Near $T^* = 1.7$, the system changes its character; effectively, the local oscillations "melt," so that the relaxation process becomes far more efficient above this temperature. This helps to understand the decreased correlations seen in Figures 4−6 for lower temperatures. It also helps to understand the long tail in Figure 4b ($T^* = 1.23$), that indexes long-time correlations,

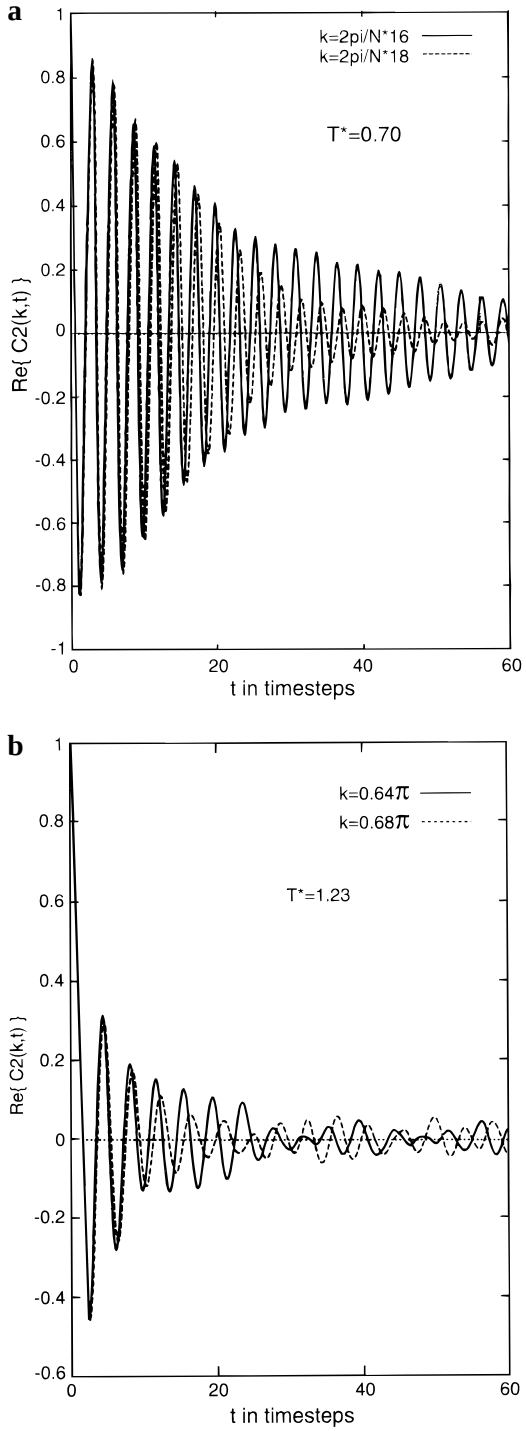

Figure 5. The Fourier time correlation function, for higher momentum. The higher momentum corresponds to greater local phase differences, and therefore the oscillations are strong even at higher temperatures ((b) shows temperature of $T^* \approx 1.23$ and (a) of $T^* \approx 0.70$).

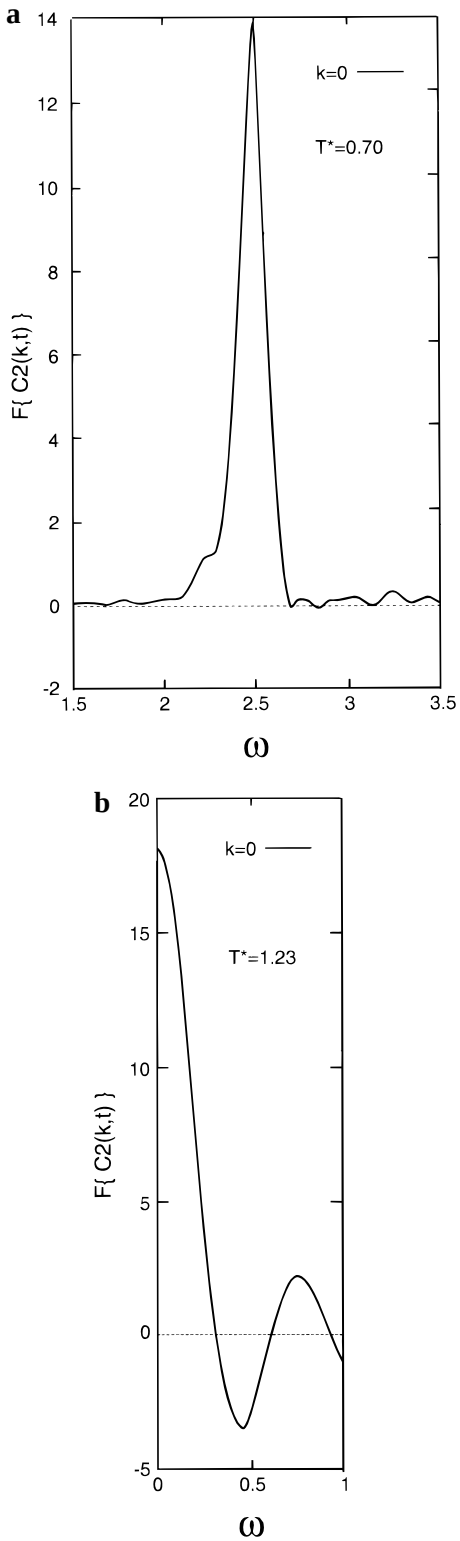

Figure 6. Fourier transforms of the momentum correlation functions. Notice that for $T^* \approx 0.70$, the Fourier transform of (a) shows a strong resonance peak; with increasing temperature, this strong peak moves to the frequency origin. The secondary peaks in (a), and the unphysical oscillation for $\omega \lesssim 3$, are noise from the Fourier analysis.

occurring near the change in the nature of the $k = 0$ peak in $C_2(k,\omega)$ from oscillatory at $T^* = 0.70$ to Rayleigh-like for $T^* = 8.74$.

The moments of the correlation functions reflect the energy relaxation and dephasing. They are defined in the usual manner:

$$\langle \omega^{2n} \rangle = \frac{\int_{-\infty}^{\infty} d\omega\ \omega^{2n} C(k,\omega)}{\int_{-\infty}^{\infty} d\omega\ C(k,\omega)} \tag{23}$$

Since for a classical system the autocorrelation functions are even functions of time the odd moments vanish. By definition $\langle \omega^{o} \rangle = 1$. It is straightforward to derive the following expression for the second moment:

$$\langle \omega^{2n} \rangle = \frac{T^*}{g(k)} \tag{24}$$

since in our units the moment of inertia $I = 1$. Here we have

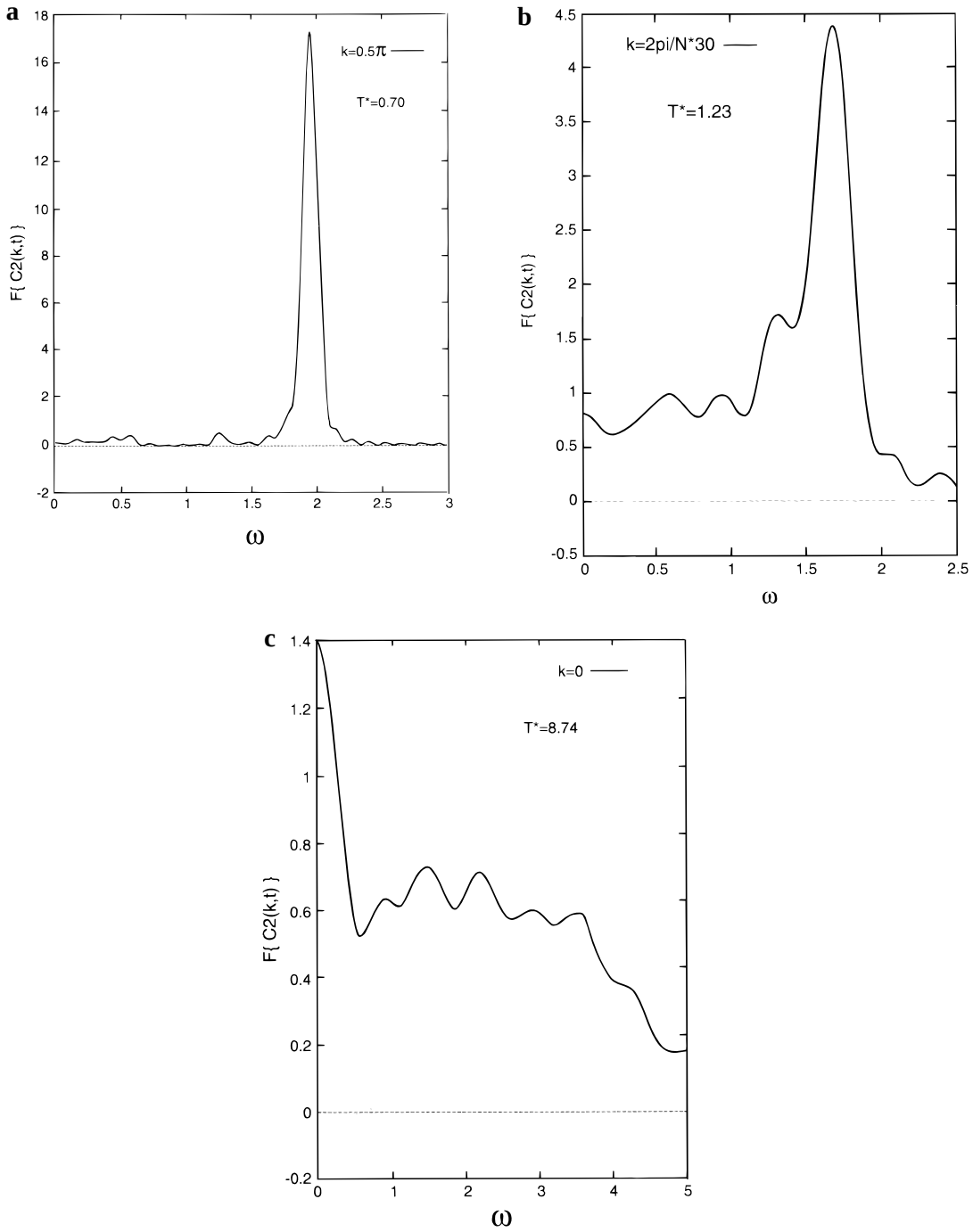

Figure 7. Fourier spectrum of the correlation function for higher momenta. Once again, one sees that on going from (a) ($T^* \approx 0.7$) to (b) ($T^* \approx 1.23$) the structure becomes smeared out as temperature increases.

introduced a wavenumber-dependent Kirkwood factor $g(k)$:

$$g(k) = 1 + \frac{1}{N}\sum_{i=1}^{N}\sum_{j=i}^{N}\langle \mu_i \cdot \mu_j \rangle / \mu^2 \qquad (25)$$

The second moment $\langle \omega^2 \rangle$ is shown as a function of the wave number in Figure 9 for different temperatures. Clearly at high temperatures the motion of the dipoles becomes uncorrelated, so that $g(k) = 1$ for all k and $\langle \omega^2 \rangle = T^*$, independent of wave length. At temperatures $T^* < 1$ (i.e., well below the transition region), $\langle \omega^2 \rangle$ reflects the dispersion relation shown in Figure 1. The moments have a maximum at $k = 0$ and fall off to a limiting value at $k = \pi$. Anharmonic behavior results in a shift of the long-wavelength ($k \rightarrow 0$) modes to lower frequency. The transition region (e.g., at $T^* = 1.23$) is characterized by a marked decrease in $\langle \omega^2 \rangle$ at long wavelengths. This reflects the slow decay of long-range orientational correlations of the dipoles as the transition region from an ordered low-temperature behavior to a highly disordered system at high temperatures is traversed. These correlations manifest themselves in a strong increase in the long wavelength limit of the Kirkwood factor $g(k = 0)$.

These correlation functions are substantially different from those observed or calculated for phonon-type systems, as is made clear in our analysis of the low energy excitations in section II. Nevertheless, there are commonalities in behavior, since the local wells in which the dipoles librate may, to a first approximation, be considered harmonic.

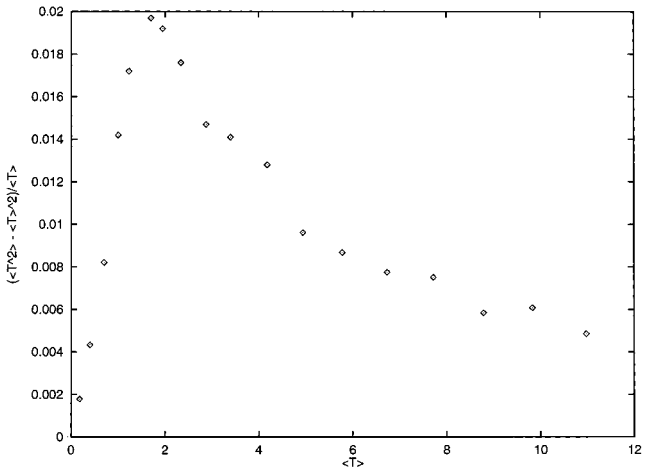

Figure 8. Fluctuations in the temperature as a function of temperature. Notice the strong peaked feature (corresponding to melting-like behavior or a peak in heat capacity) near $T^* \approx 1.7$.

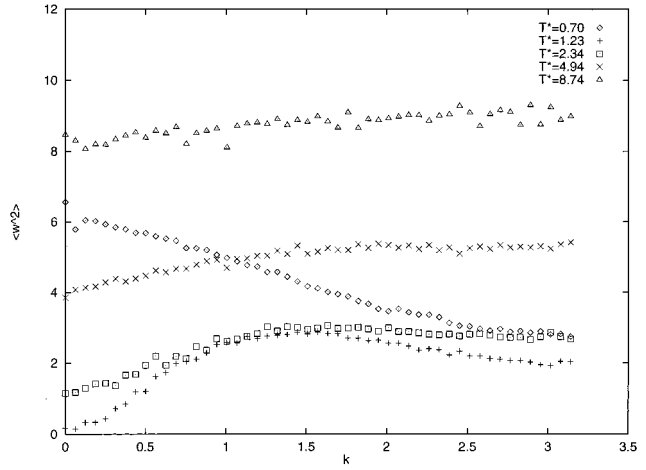

Figure 9. The temperature dependent second moment of the correlation function, defined by eq 23. At very high temperatures, all correlations are unimportant and the even frequency moments are essentially independent of wave vector. For very low temperatures, the behavior is essentially that of the dispersion relations for the chain, of eq 14 and Figure 1. At intermediate temperatures, a substantial reduction in the long wave length part of the second moment is due to orientational correlations, as the order of the array is being destroyed. Near $T^* = 1.7$ (peak in Figure 8 corresponding to melting), the $k = 0$ component reflects a critical slowing of long-wavelength correlation.

V. Remarks and Speculations

The rapid progress made in molecular assembly techniques provides an opportunity to consider the response of structured molecular arrays of various kinds. Here we have considered a very simple structure, corresponding to rigid molecular dipoles, whose centers are rigidly positioned with respect to one another. We have examined the dispersion relations, the low-energy excitations, the dissipation of initially excited single dipole, and the nature of the dynamics and correlations in the chain of dipoles.

This model system has been studied partly because of recent synthetic work that is indeed preparing molecular rotators that can be positioned in either linear or planar motifs. The interaction among these molecular rotors will, when they are far separated, be of electrostatic dipole−dipole type. When the rotors are brought closer together, steric interactions may become more important, and one might expect some very interesting locking behavior, when the steric overlaps become such that very strong local correlations are required for any actual rotation to occur. This limit is substantially more complicated than the simple electrostatic one considered here.

One reason for this simulation is the possibility of energy transfer between, say, colliding gas molecules and the dipolar array. In section III, we saw that even strong local excitation will damp out relatively rapidly into delocalized librations and that the reflection from walls might well be seen; this latter behavior has also been seen in vibrational relaxation simulations, both classical and quantal.

Physically, the current results contain four significant messages: 1. The low-energy dispersion relation (eq 14) for this dipolar chain resembles the optical phonon (Figure 1). 2. For impulsive rotational excitation of an initial dipole, the excitation travels down the chain and reflects from the chain end. Longer chains will echo more slowly, as quantitatively given by the theoretical group velocity (eq 16, Figures lb and 2c). 3. Thermal behavior shows a melting-like transition at temperature equivalent to the local rotational barrier ($T^* \sim 1.7$; Figure 8). 4. The dynamics show nonmonotonic behavior, especially at long wavelength. As temperature increases, the local dipoles shift from a resonant response for temperature well below the melting transition to a narrow Rayleigh peak at the transition to a broadened response for high temperature.

The problem of rotation about the z-axis (in the (x,y) plane), rather than in a plane containing the z-axis (the (x,z) plane), begins with the Lagrangian

$$L = {}^1/_2 I \sum_i \dot{\varphi}_i^2 - {}^1/_2 {\sum_{ij}}' \frac{\mu^2}{r_{ij}^3}(\cos\varphi_i \cos\varphi_j + \sin\varphi_i \sin\varphi_j) \tag{26}$$

in place of eq 2. This system, which will be analyzed elsewhere, has very different excitation properties than does the in-plane rotation analyzed in the present work; it corresponds to a classical version of the (x,y) model.[19]

The dispersion relations and thermal behaviors observed here should be observable using scattering methods (atom scattering, light scattering, neutron scattering) on properly prepared structures. More interesting, perhaps, is the electromagnetic interaction that might be expected. Spectroscopically, for structure **A**, the relatively larger moment of inertia I yields a resonance (Figure 6a) in the giga Hertz regime (see part 3 of the appendix); smaller I would blue shift this peak. Rotating dipoles generate electro-magnetic radiation, and if the dipoles are rotating, such an array of dipoles may act as an electromagnetic generator. Studies of this possibility are beginning.

Acknowledgment. This work was supported by grants from NSF (Grant CHE-9318469, to J.M.), ONR (Grant N00014-97-J-1684, to M.R.), and SON (to S.D.L.). We thank the referee of a preliminary version for some useful suggestions.

Appendix

Details of the MD Simulations. *1. The Simulation.* Using the constrained Lagrangian

$$L^* = \frac{1}{2\mu^2}\sum_{i=1}^{N} I\dot{\tilde{\mu}}_i^2 - \sum_{i=1}^{N-1}\sum_{j=i+1}^{N}\left(\frac{\tilde{\mu}_i\cdot\tilde{\mu}_j}{r_{ij}^3} - 3\frac{(\tilde{\mu}_i\cdot\tilde{r}_{ij})(\tilde{\mu}_j\cdot\tilde{r}_{ij})}{r_{ij}^5}\right) + {}^1/_2\sum_{i=1}^{N}\lambda_i(\tilde{\mu}_i^2 - \mu^2) \tag{A1}$$

and applying the Euler−Lagrange equation

$$\frac{\mathrm{d}}{\mathrm{d}t}\left(\frac{\partial L^*}{\partial \dot{\tilde{\mu}}_i}\right) - \frac{\partial L^*}{\partial \tilde{\mu}_i} = 0, \qquad i=1,...,N \tag{A2}$$

gives

$$\frac{1}{\mu^2} I \ddot{\tilde{\mu}}_i^2 = -\sum_{\substack{j=1 \\ j\neq i}}^{N} \left(\frac{\dot{\tilde{\mu}}_j}{r_{ij}^3} - 3\frac{r_{ij}(\tilde{\mu}_j \cdot \tilde{r}_{ij})}{r_{ij}^5} \right) + \lambda_i \tilde{\mu}_i \tag{A3}$$

Differentiating the constraint $\tilde{\mu}_i^2 - \mu^2 = 0$ two times with respect to the time gives $\dot{\tilde{\mu}}_i^2 + \tilde{\mu}\ddot{\tilde{\mu}}_i = 0$ which is used to eliminate $\ddot{\tilde{\mu}}_i$, thus giving an expression for λ_i:

$$\lambda_i = \frac{1}{\tilde{\mu}_i^2}\left[\sum_{\substack{i=1 \\ j\neq i}}^{N} \left(\frac{\tilde{\mu}_i \cdot \tilde{\mu}_j}{r_{ij}^3} - 3\frac{(\tilde{\mu}_i \cdot \tilde{r}_{ij})(\tilde{\mu}_j \cdot \tilde{r}_{ij})}{r_{ij}^5} \right) - \frac{\dot{\tilde{\mu}}_i^2 I}{\mu^2} \right] \tag{A4}$$

Inserting this into the expression for $\ddot{\tilde{\mu}}_i$ we have the equations of motion for the dipoles. These are solved by applying the Gear predictor−corrector method.

Constraints are corrected assuring that

$$\tilde{\mu}_i^2 = \mu^2 \qquad \text{and} \qquad \tilde{\mu}_i \cdot \dot{\tilde{\mu}}_i = 0$$

2. Temperature. On the basis of equipartition,

$$\frac{1}{2\mu^2} \sum_{i=1}^{N} I \dot{\tilde{\mu}}_i^2 = {}^1/_2 NkT, \tag{A5}$$

which holds at sufficiently high T. We define a reduced temperature by

$$T^* = \frac{kT}{\epsilon} = \frac{\frac{I}{N}\sum_{i=1}^{N} \dot{\tilde{\mu}}_i^2}{\frac{\mu^4}{r_o{}^3}} = \frac{I r_o{}^3}{N\mu^4} \sum_{i=1}^{N} \dot{\tilde{\mu}}_i^2 \tag{A6}$$

3. Units. For typical chromophores of interest, such as the chiral Re complexes calculated by Michl's group (for example, **A**), the actual moment of inertia $I \sim 10^{-36}$ g cm^2. Typically, the separation r_o might be 25 Å and the dipole moment $\mu \cong 60$ D. Then $\epsilon = \mu^2/r_o{}^3 \cong 1100$ cm^{-1}. For such molecules, then $T = \epsilon T^*/k = T^*$ (1500 K), and the value $T^* = 1.7$ of Figure 8, near which the excitation instability occurs, is roughly at $T =$ 2500 K, which is clearly experimentally unapproachable. If r_o were doubled, however, this becomes $T^* \cong 300$ K.

The unit of energy in Figure 2 is $\mu^2/r_o{}^3 = \epsilon \cong 1100$ cm^{-1}. The total initial energy in Figure 2 would then be 13700 cm^{-1}.

The units of time are scaled by the moment of inertia I. If we define a dimensionless time θ by $t = \theta\,(Ir_0{}^3/\mu^2)^{1/2}$, then one unit of θ will be $(Ir_0{}^3/\mu^2)^{1/2}$ units of time. The equations of motion (eq A.3) can be rewritten in terms of this dimensionless time θ, and all results in the body of the paper are given in units of θ.

For a chromophore such as A, for which I is of order 10^{-36} g cm^2, if $r_o \cong 25$ Å, $(Ir_0{}^3/\mu^2)^{1/2}$ is about 4×10^{-9} s. Thus the time unit of this paper, for such chromophores separated by 25 Å, is roughly 4 ns.

4. Initial Configuration of the Dipoles. Initially all dipoles are aligned,

$$\dot{\tilde{\mu}}_i = \mu \begin{pmatrix} 1 \\ 0 \end{pmatrix}$$

and they are given random velocities:

$$\dot{\tilde{\mu}}_i = \mu \begin{pmatrix} 0 \\ v_i \end{pmatrix}$$

where $v \in [-1; 1]$. Different temperatures are achieved by scaling all velocities by the same number. Initially the sum of all velocities is zero.

References and Notes

(1) Tieke, B. *Adu. Mater*. **1990**, *2*, 222.
(2) Whitesides, G. M.; Mathias, J. P.; Seto, C. T. *Science* **1991**, *254*, 1312.
(3) Lindsay, J. S. *New J. Chem.* **1991**, *15*, 153.
(4) McGrath, K. P.; Kaplan, D. L. *Mater. Res. Soc. Symp. Proc.* **1994**, *330*, G1.
(5) Ulman, A. *An Introduction to Ultrathin Organic Films*; Academic Press: New York, 1991.
(6) Dubois, L. J.; Nuzzo, R. G. *Annu. Rev. Phys. Chem.* **1992**, *43*, 437.
(7) Maoz, R.; Sagiv, J. *J. Colloid Interface Sci.* **1984**, *100*, 465.
(8) Li, D.; Ratner, M. A.; Marks, T. J.; Zhang, L.; Yang, T.; Wong, G. *J. Am. Chem. Soc.* **1990**, *112*, 7389.
(9) *Modular Chemistry*; Michl, J., Ed.; NATO ASI Series 499; Kluwer: Dordrecht, 1997.
(10) Michl, J. In *Applications of Organometallic Chemistry in the Preparation and Processing of Advanced Materials*; Harrod, J. F., Laine, R. M., Eds.; Kluwer: Dordrecht, 1994.
(11) Kaszynski, P.; Friedli, A. C.; Michl, J. *J. Am. Chem. Soc.* **1992**, *114*, 601.
(12) Michl, J. In *Chemical Synthesis: Gnosis to Prognosis* Chatgilialoglu, C., Snieckus, V., Eds.; Kluwer: Dordrecht, 1996.
(13) Harrison, R. M.; Magnera, T. I.; Vacek, J.; Michl, J. In *Modular Chemistry*; J. Michl, ed.; Kluwer: Dordrecht, 1997; p 1. Vacek, J.; Michl, J. *New J. Chem.* **1997**, *21*, 1259.
(14) Pietro, W.; Marks, T. J.; Ratner, M. A. *J. Am. Chem. Soc.* **1985**, *107*, 5387. Hiejima, T.; Yakushi, K. *J. Chem. Phys.* **1995**, *103*, 3960.
(15) For example, see: Madelung, O. *Introduction to Solid-State Theory*; Springer: Berlin, 1981; pp 165 ff.
(16) Abramowitz, M.; Stegun, I. A. *Handbook of Mathematical Functions*; Dover: New York, 1965; pp 807 ff.
(17) For example, see: Ziman, J. *Principles of The Theory of Solids*; University of Cambridge Press: Cambridge, 1965; p 49.
(18) Reference 15, pp 129 ff.
(19) For example, see: Stanley, H. E. *Introduction to Phase Transitions and Critical Phenomena*; Oxford University Press: Oxford, 1991.